

Chapter 4

Numerical Simulation of Coastal Sediment Transport by the 2011 Tohoku-Oki Earthquake Tsunami

Daisuke Sugawara and Tomoyuki Takahashi

Abstract Erosion and deposition by the 2011 Tohoku-oki tsunami in the coastal areas of the Sendai Plain were numerically investigated using the tsunami sediment transport model (STM). The simulation suggested that much of the sediment deposited on land originated from the beach and dune, whereas the contribution from sea-bottom sediments was quite minor. Erosion observed at the backs of engineering structures such as reinforced concrete (RC) dikes was reproduced well in the simulation. Simulated deposition and erosion inside the nearby coastal forest and farmlands were generally consistent with the observed data. Further investigation of the model parameters and implementation of dynamic change in the roughness coefficient and destruction of the structures are required to simulate detailed local variability of erosion and deposition and of the thin sand layer in the inland areas.

Keywords Numerical modeling • Sediment transport • Tsunami deposit

4.1 Introduction

Tsunami deposits have been widely used for identifying past large-scale tsunamis and assessing the magnitudes of paleotsunami events. Recent studies have attempted to estimate tsunami height and flow speed based on sedimentary data, such as the thickness and grain size of deposits. Tsunami erosion and deposition can be calculated by the sediment transport model (STM) developed by Takahashi et al. (2000). The model simulates bathymetric and topographic changes under given flux and bottom shear conditions. The STM has been validated using modern examples prior

D. Sugawara (✉)

International Research Institute of Disaster Science, Tohoku University,
Sendai, Japan
e-mail: sugawara@irides.tohoku.ac.jp

T. Takahashi

Faculty of Safety Science, Kansai University, Takatsuki, Japan

to being applied to paleotsunami events. For example, Gusman et al. (2012) recently applied the model to sedimentation caused by the 2004 Indian Ocean tsunami at Lhok Nga, Banda Aceh, Indonesia. They showed that the model reasonably reproduced the thickness distribution of the sand layer found in the field and suggested that the STM can be applied to numerical investigation of the source process of large tsunamis. If this is so, the magnitudes of the paleotsunami events can be quantified based on paleotsunami deposits. The 2011 Tohoku-oki tsunami offers a valuable opportunity for validation of the STM. An abundance of sedimentary data, as well as measurements, video footage and eyewitness accounts, are available for the tsunami.

However, recent studies of the Tohoku-oki tsunami deposits from the coastal plains have revealed a number of specific sedimentological features. The distribution of the sandy deposit was typically limited to within 57–76 % of the inundation distance (e.g., Abe et al. 2012). Beach sand and dune soil have been estimated to be the main source of the tsunami deposits found in the zone up to 1 km from the shoreline, and only a small contribution of marine sediments has been detected based on grain-size and paleontological analysis (Szczeniński et al. 2012). Engineering structures, such as reinforced concrete (RC) dikes, are considered to have played an important role in sediment transport. Marked scouring and erosion at the backs of such structures were commonly observed in the study area (e.g., Richmond et al. 2012). Some of the RC dikes installed at the coast were severely damaged and collapsed. Hydraulic jump on the back of the structures is attributed to the intensive erosion of sediments and loss of the foundations of the structures (Tappin et al. 2012). It is likely that natural and anthropogenic coastal topographic features may have contributed to the limited distribution of the sand and the faint marine signature in the tsunami deposits.

In the present study, a numerical simulation of sediment transport caused by the 2011 Tohoku-oki earthquake tsunami was performed using the STM to reproduce and investigate the change of the coastal geomorphology of the Sendai Plain in northeast Japan (Fig. 4.1a, b). The performance of the model was validated using an available high-resolution digital elevation model (DEM) and field data on erosion and deposition caused by the tsunami.

4.2 Materials and Method for Simulation

4.2.1 Topography Data for Simulation

The computational domain from the open ocean to the Sendai Plain was covered by a nesting grid system. The tsunami generation and propagation was calculated on the coarser grids with spatial resolutions (dx) of 405, 135, 45 and 15 m. In the study area, a pre-tsunami DEM with $dx = 5$ m is available (Fig. 4.1b) and was used for the calculation of the STM. Elevations of the engineering structures with paved surfaces, such as roadways and RC dikes, are well reproduced in the DEM. The elevation was surveyed by the Geospatial Information Authority of Japan in

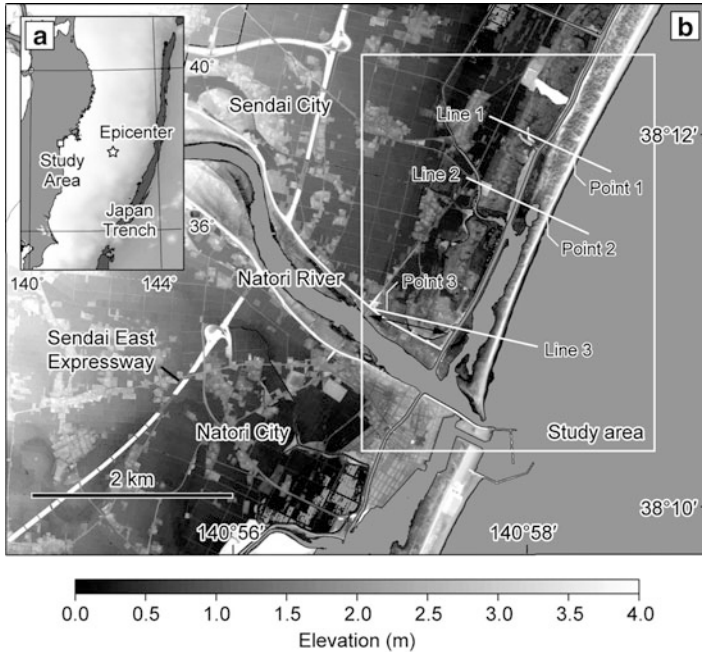


Fig. 4.1 Location map of the study area (a) and pre-tsunami topography of Sendai Plain and the study area (b)

the winter season of 2005–2006, nearly 5 years before the Tohoku-oki tsunami. Some recent topographic changes, such as a slight retreat of beach, implementation of new roadways and land development, which have occurred since 2006, are not incorporated in the DEM.

Manning's roughness coefficient, n , is an important parameter in the calculation of flow speed and bottom shear. A land use map was developed based on the aerial photographs (Fig. 4.5). A value for Manning's roughness coefficient was assigned to each grid cell on the basis of the land use map and findings by Kotani et al. (1998). In the simulation, engineering structures with paved surfaces are distinguished using the land use map. Although some of the structures were severely damaged and collapsed, they were not the main source of the tsunami deposits. The paved structures were not directly eroded by tsunami flow but rather collapsed due to erosion of their foundations. Some of the RC dikes might have been damaged directly by the impact of the tsunami wave. The STM in its present form cannot treat such dynamic and complex processes as the destruction of these structures. Thus, the paved surfaces were assumed to be intact during the computation. Erosion of the sediments does not extend below the elevations of these features. In addition, surfaces with muddy sediments, such as dry fields and rice paddies, were also assumed to be intact during the computation. This assumption was made because the present study was focused on the transport of sand. As noted in Sect. 4.2.2, the surficial sediments of these farmlands were in fact eroded. However, they did not contribute to the thickness of sand erosion and deposition.



Fig. 4.2 Erosion at the back of the reinforced concrete dike at Point 1 in Fig. 4.1b

4.2.2 Observed Data for Validation

A post-tsunami DEM with $dx = 5$ m is available for the study area. The survey was carried out immediately after the tsunami (during 19–23 March 2011), although most of the lowland was still flooded at that time. The vertical precision of the pre- and post-tsunami DEMs is around ± 15 cm. The post-tsunami DEM may include the elevation change due to the accumulation of debris. The data was processed by eye, and the debris greater than 1 m in height and 10–20 m in length was removed. Coseismic subsidence of 20–30 cm was observed in the study area (Ozawa et al. 2011). Because the Sendai Plain is alluvial in origin, the surficial sediments of the study area are composed of unconsolidated sediments of natural levees, beach ridges and back marshes (Matsumoto 1985). Local subsidence due to liquefaction was observed at many locations in the study area. A correction was made for this local subsidence based on flat areas with compacted or paved surfaces, such as schoolyards outside of the tsunami inundation area, which serve as reference levels for tsunami erosion and deposition. Taking into account the local subsidence that occurred, coastal elevation change between the pre- and post-tsunami DEMs was assumed to be an approximation of tsunami-induced topographic change. Detailed comparison of the deposition and erosion base in the DEMs is difficult, particularly if the erosion is shallow and/or deposition is thin, because of the limit of the precision of the survey and the correction for local subsidence.

Topographic changes and damage to engineering structures were observed in the field on 5 June 2011 (Points 1 and 2 in Fig. 4.1b).

In Sendai, RC dikes with typical heights of 5–6 m were installed on the sand dunes. At Point 1, the RC dike was still present. Severe erosion was observed at the back of the RC dike, and the depth of the erosion was up to 2–3 m at this location (Fig. 4.2). At Point 2, the dike was totally destroyed (Fig. 4.3). A considerable number of tetrapods and concrete casts were scattered on the beach and transported



Fig. 4.3 Collapsed RC dike and erosion of the sand bar at Point 2 in Fig. 4.1b. Concrete casts that comprised the dike were scattered and buried by sand

inland and even buried by beach sand. Although the pre-tsunami coastline extended further south of this location, the post-tsunami coastline was terminated due to the massive erosion of the beach.

The tsunami deposit was investigated on 26 May 2011 at 16 pits along the inland part of Line 3 (Fig. 4.1b). The observation pits were arranged at 50-m intervals. The area was originally used for farmland, such as dry fields and rice paddies. The tsunami deposit was composed of a coarse- to medium-grained sand layer, capped by a thin (approximately 1 cm) mud layer (Fig. 4.4). The thickness of the sand layer varies significantly from nearly 0 to 15 cm. The sand layer was clearly in contact with the underlying muddy soil and included many rip-up clasts entrained from the soil. This suggests that severe erosion might have taken place prior to the deposition of the sand layer (Fig. 4.5).

4.2.3 Method of Calculation

The STM was coupled with a tsunami propagation and inundation model based on nonlinear shallow-water theory (TUNAMI-N2; Goto et al. 1997; IOC/IUGG TIME Project). The simulation reproduced offshore tsunami generation, propagation to the coast and inundation for three model hours. Source models for the Tohoku-oki tsunami have been investigated in a number of studies. A composite fault model proposed by Japan Nuclear Energy and Safety Organization (JNES 2011) was used for the tsunami source. The model was developed based on the inversion analysis of tsunami records from tide gauges and GPS buoys, taking into account the tsunami heights measured near the coast and the observed coseismic subsidence on land. Crustal deformation by the fault movement was calculated using the method developed by Okada (1985). The subsidence calculated from the fault model approximates the observed data well (JNES 2011).

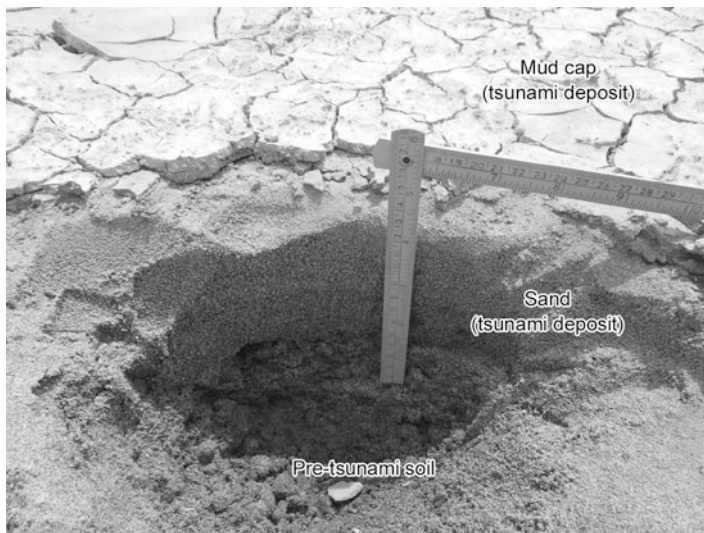


Fig. 4.4 Tsunami deposit found at Point 3 in Fig. 4.1b. The deposit was 12 cm thick and composed mainly of medium-grained sand capped by a thin mud layer

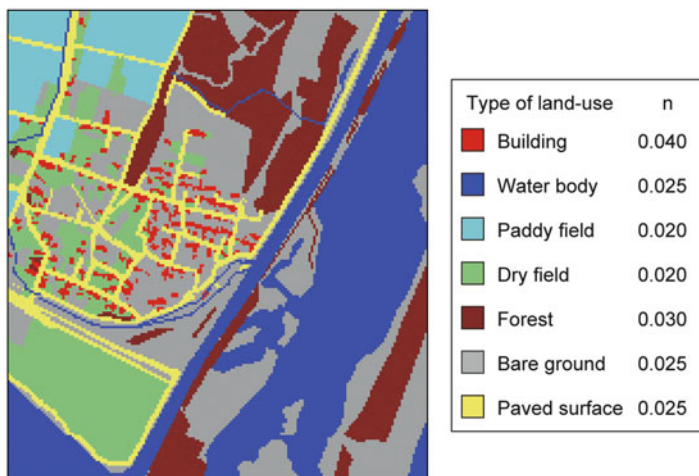


Fig. 4.5 Example of the land use map used in the present study. n : Manning's roughness coefficient. Buildings, paddy fields, dry fields and paved surfaces were assumed to be intact during the computation

The STM assumes two distinct layers of bed load and suspended load and assumes exchange between the two layers. Details of the model are given by Takahashi et al. (2000) and Gusman et al. (2012). Two key parameters control the behavior of the STM, namely, the grain size (d) and the saturated concentration of the suspended load (C_s). Previous studies documented that most beach and dune sands from the Sendai Plain are composed of fine- to medium-grained sand with a mean diameter of 2ϕ (0.25 mm) (e.g., Matsumoto 1985). A uniform grain size of

$d = 0.25$ mm was assumed in the present study. Takahashi et al. (2011) found that the coefficients for the pick-up rate equations for the bed and suspended loads depend on the grain size. The grain-size-dependent parameters for the pick-up rate equations were chosen based on Takahashi et al.'s description of their findings. The saturated concentration of the suspended load (C_s) was introduced to the STM to maintain numerical stability during extreme flow conditions, such as at the bore front. In a previous study, Gusman et al. (2012) used a value of $C_s = 1\%$ in their calculations and obtained good agreement between simulated and observed results. Although there is still some uncertainty associated with the physical model and reasonable determination of the parameter (Takahashi 2012), a value of $C_s = 1\%$ was assumed in the present study.

4.3 Results and Discussion

4.3.1 General Topographic Change

Figure 4.6 shows a comparison of the simulated (A) and observed (B; the post-tsunami DEM) topography of the study area. Note that the simulation shows the

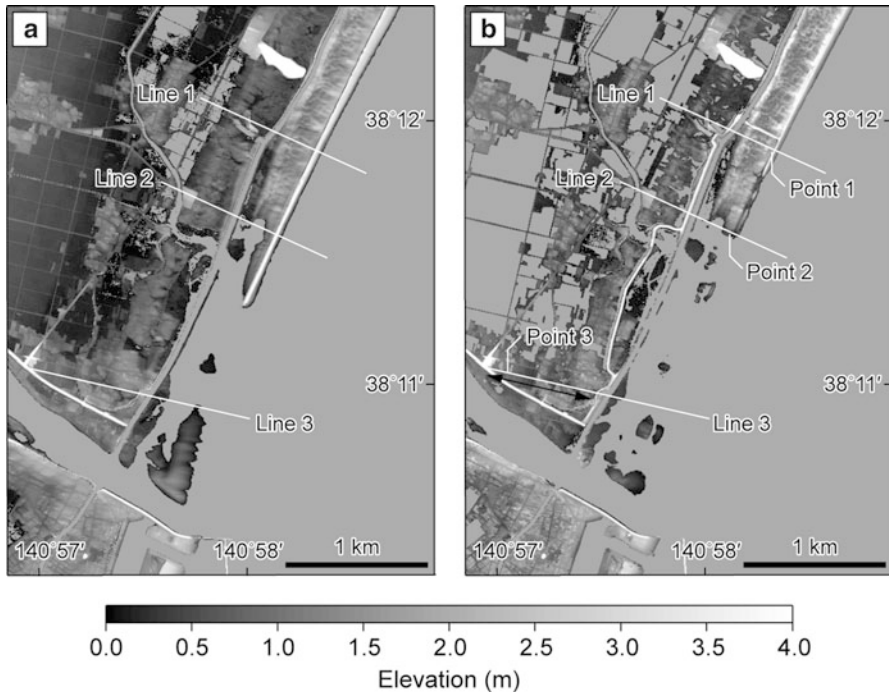


Fig. 4.6 Comparison of (a) simulated and (b) observed elevations. Note that elevations of the lowlands were not measured because of the flood water resulting from the tsunami. Surfaces covered by water are colored a plain gray

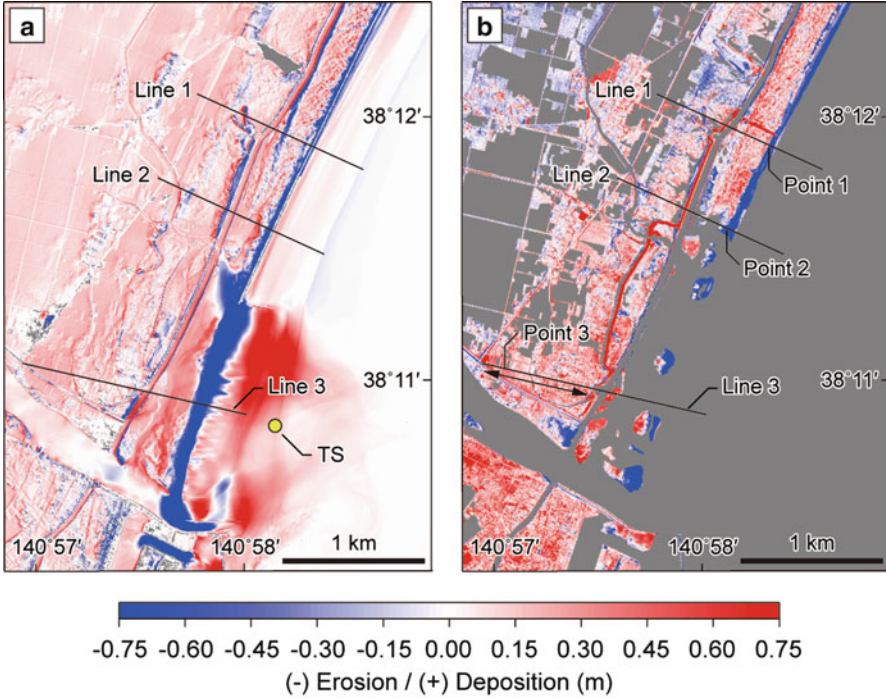


Fig. 4.7 Comparison of (a) simulated and (b) observed elevation changes. The line with arrows at both ends in (b) shows the location of the field survey of tsunami deposits

topography 3 h after the earthquake (nearly 2 h after the tsunami attack), and the observation was made at least 8 days after the tsunami. Subsequent tsunami waves more than 3 h later and normal wind waves might have changed the topography.

Before the tsunami, a sand bar and a lagoon (Ido-ura) were situated in the north of the mouth of the Natori River (Fig. 4.1b). The sand bar was not protected by RC dikes, except for the northern part. The post-tsunami DEM shows that the sand bar was severely eroded and the lagoon was connected directly to the open sea (Fig. 4.6b). In general, the simulation reproduced the massive erosion of the sand bar well, although the remaining area at the south was greater in the simulation. A significant difference between the simulation and observation can be observed at the north section of the sand bar (Figs. 4.6a, b), where an RC dike was installed (Fig. 4.3). In fact, the dike collapsed due to the tsunami, and this may have caused the massive erosion of the sand bar. The erosion in the simulation was more moderate than that observed because in the simulation the RC dike remained intact.

Figure 4.7 shows a comparison of the simulated (A) and observed (B) bathymetric and topographic changes in the study area. Note that bathymetric change is not included in the observed data. Both the simulation results and the observed data showed that the erosion on land was greatest near the beach and on the sand bar.

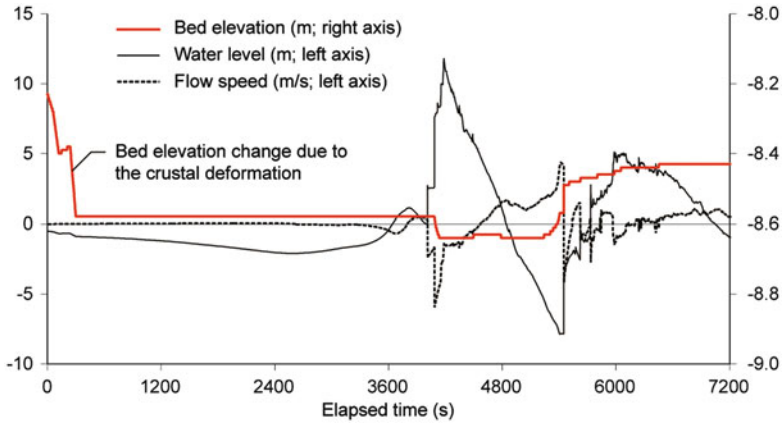


Fig. 4.8 Time series of the bed elevation, water level and flow speed at 500 m offshore of the sand bar (TS in Fig. 4.7). Note that the positive value of flow speed indicates eastward (seaward) flow direction, and the negative value corresponds to westward (landward) flow direction

Figure 4.8 shows a time series of bed elevation, water level and flow speed at 500 m offshore of the sand bar. At this location, the sea bottom was eroded by the first positive wave. The timing of the erosion is associated with the peak of flow speed at 4,100 s, rather than the maximum of the water level, which was delayed nearly 100 s. The bed level was recovered in the last 200 s of the negative wave, and even become higher than the original elevation. The simulation results suggest that most of the sediments that comprised the sand bar were washed out and deposited within 1 km offshore of the coastline, and some of the sediments were deposited in the lagoon. This implies that the total erosion of the sand bar is primarily explained by backflow. In the simulation, minor erosion of the sea bottom occurred approximately 500 m offshore of Lines 1 and 2 (Fig. 4.7a). This suggests that a quite small amount of marine sediment was transported and deposited onshore, which is consistent with findings from recent research on the region near the study area (e.g., Szczuciński et al. 2012).

4.3.2 Erosion at the Backs of RC Dikes

Comparisons of the elevations and their tsunami-induced changes along Lines 1 and 2 (Fig. 4.1b) are shown in Figs. 4.9 and 4.10. The elevation of the RC dike on Line 1 was approximately 4 m (Fig. 4.9a). According to the topographic change estimated from the pre- and post-tsunami DEMs, the erosion at the back of the dike reached more than 1.5 m (Fig. 4.9b); meanwhile, the depth of the erosion was estimated to be up to 2–3 m in field observations (Fig. 4.2). The simulation estimated erosion up to 2.5 m at this location. The difference in these results can

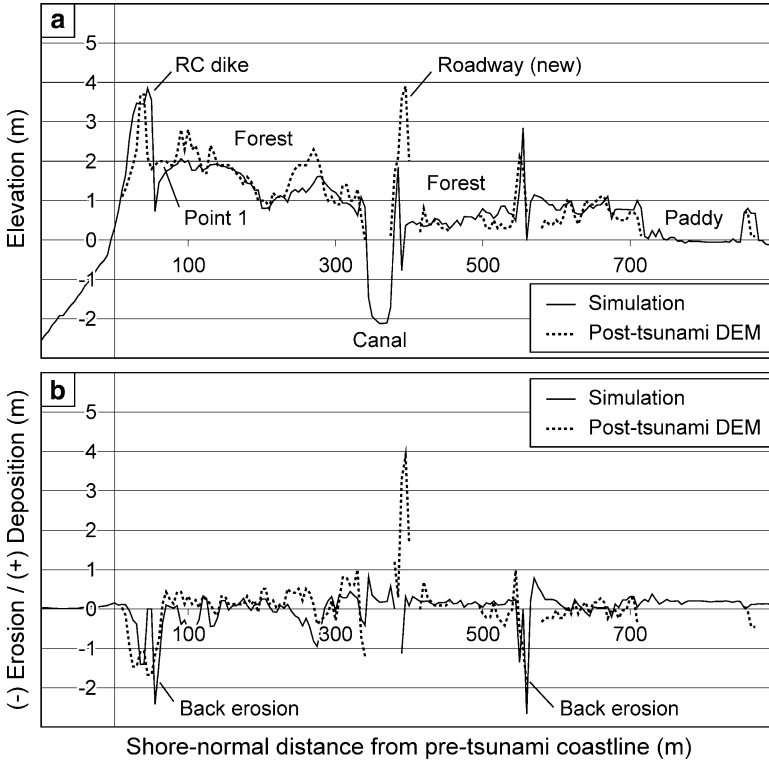


Fig. 4.9 Comparison of simulated and observed (a) elevation and (b) erosion and deposition along Line 1 in Fig. 4.1b

be attributed to a numbers of factors, such as the parameters applied to the tsunami and sediment transport models, post-tsunami reworking of sediments and precision of the surveying. Nonetheless, the simulation generally reproduced the deep excavation at the backs of the dikes.

The differences in elevation and its tsunami-induced changes are significant at locations where an RC dike collapsed. The elevation of the dike on Line 2 was 5.5 m (Fig. 4.10a), and the erosion at the back of the dike predicted in the simulation approached 3.5 m (Fig. 4.10b). In fact, the RC dike was severely damaged and the sand bar was flattened along Line 2 (Fig. 4.3). Compared to the RC dike along Line 1, it is obvious that deeper erosion occurred at the back of the higher RC dike along Line 2. This may have led to loss of foundation support and total collapse of the dike, such as described by Tappin et al. (2012). In Fig. 4.10, the differences in the simulated and observed elevations (A) and their change (B) are significant at least 300 m from the coastline. This suggests that the protective effect of the dike would have extended to this distance if the dike could have withstood the tsunami impact.

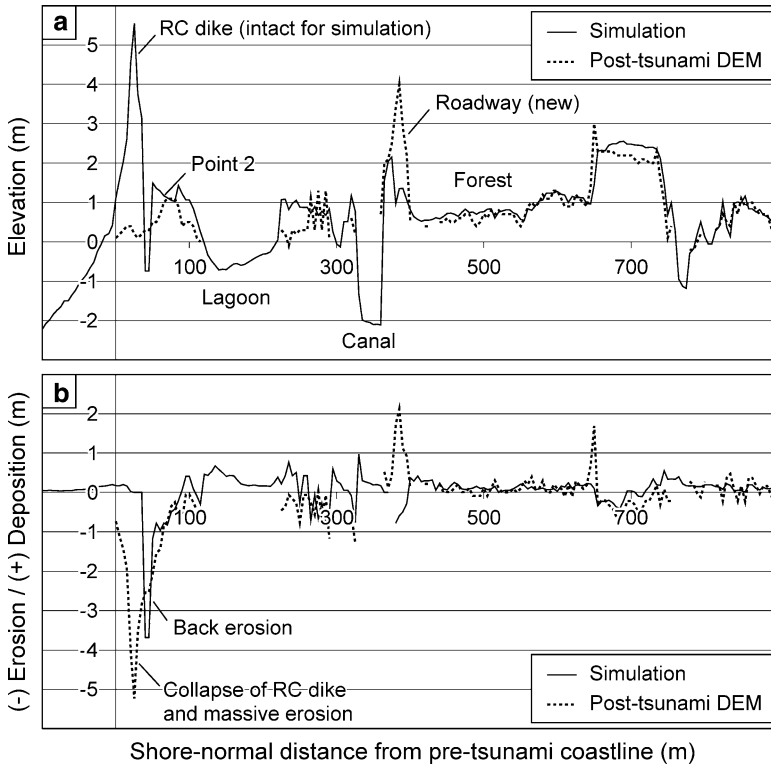


Fig. 4.10 Comparison of simulated and observed (a) elevation and (b) erosion and deposition along Line 2 in Fig. 4.1b

4.3.3 Detailed Comparison of Erosion and Deposition

In the study area, coastal forests of pine trees covered the zones from the backs of the dikes up to 600 m from the beach. Both erosion and deposition can be observed in the simulation and observation (Fig. 4.7), and the profiles of the elevation and its changes are generally consistent between the simulation and the observation (Figs. 4.9 and 4.10). However, the distribution patterns of the elevation changes are slightly different. For example, the difference in the elevation along Line 1 is significant at approximately 100 and 250 m from the coastline (Fig. 4.9). The simulation indicated that erosion up to 0.5–1.0 m occurred, whereas the observation showed that deposition dominated at these locations. This discrepancy occurred because a uniform value of Manning’s roughness coefficient of $n = 0.040$ was assumed in the simulation for the coastal forest. In fact, the age, height and density of the trees varies from place to place. In addition, the trees in this area were broken or uprooted and flattened during the tsunami attack. Actual frictional resistance to flow and the capacity for sediment transport would have varied in terms of time and space. To reproduce in detail

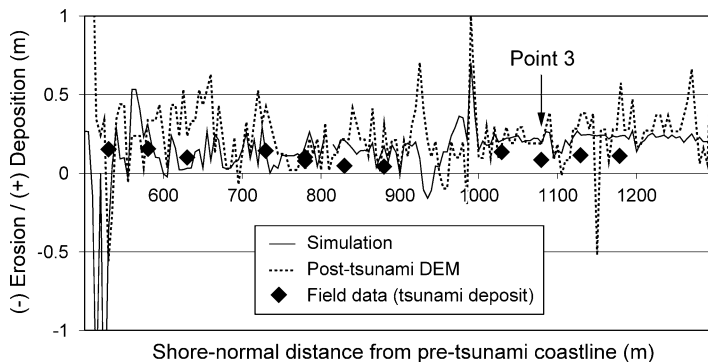


Fig. 4.11 Comparison of simulated and observed deposition and erosion along Line 3 in Fig. 4.1b

the topographic change of a densely vegetated area, local and temporal variation of the roughness coefficient should be included in the STM.

Figure 4.11 shows the erosion and deposition along the part of Line 3 that extends from 500 to 1,200 m inland of the coastline. Erosion and deposition estimated from the pre- and post-tsunami DEMs showed significant fluctuations in this section. This may be attributable to the precision of the surveying, as well as to the inclusion of tsunami debris. It is difficult to make a reasonable comparison for this line using the DEMs. The actual deposition measured in the field approached 15 cm and was thinnest approximately 800–1,000 m from the coastline. The thickness of deposition according to the simulation was comparable to that measured in the field data for some locations; however, the simulation generally overestimated the measured values.

In particular, in the section 1,000–1,200 m from the coastline, where the measured deposition was approximately 10 cm, the simulated deposition exceeded 20 cm, twice the field-measured thickness. As mentioned in Sect. 4.3.2, the difference can be explained by a numbers of factors, although post-tsunami reworking of sediments would not have taken place because the sand layer was capped by a mud layer deposited from suspension during the stagnation period of the tsunami flooding. Although the thickness of the tsunami deposition found after the Tohoku-oki tsunami approached 30 cm near the beach, it suddenly decreased to 15 cm at a distance 1 km inland of the coastline. At the landward limit of the distribution, the thickness of the sand layer thinned from a few centimeters to a few millimeters (Abe et al. 2012). Takahashi (2012) noted that the concentration of suspended load estimated by the STM is sensitive to the flow speed derived from the tsunami inundation model and the parameterization of the saturation of the suspended load. Simulation of tsunami deposition in inland areas may require additional research on the model parameters involved, such as Manning's roughness coefficient, n , the saturated concentration of the suspended load, C_s , and grain-size-dependent coefficients of the pick-up rate equations.

4.4 Conclusions

We conclude that the tsunami sediment transport model (STM) can be applied to the erosion and deposition by the Tohoku-oki tsunami. The simulated erosion on the sand bar and at the backs of the RC dikes was consistent with observations, and the eroded sediments could have been the main source of the tsunami sediments deposited inland. To simulate deposition and erosion in coastal forests, spatial and temporal change of the roughness coefficient needs to be implemented in the STM. Application of the STM to the formation of thin tsunami-deposited layers (less than 30 cm) inland requires further research on the model parameters.

Acknowledgments We acknowledge the Tohoku Regional Bureau, Ministry of Land, Infrastructure and Transport, for providing the post-tsunami digital elevation model of the study area. We wish to thank Mr. Shunji Iwama, for his efforts in making the land use map. The research was financially supported by and carried out as a part of the Strategic Program for High-Performance Computing Infrastructure sponsored by the Ministry of Education, Culture, Sports, Science and Technology in Japan.

References

- Abe T, Goto K, Sugawara D (2012) Relationship between the maximum extent of tsunami sand and the inundation limit of the 2011 Tohoku-Oki tsunami on the Sendai Plain. *Sed Geol* 282:142–150. doi:10.1016/j.sedgeo.2012.05.0049
- Goto C, Ogawa Y, Shuto N, Imamura F (1997) Numerical method of tsunami simulation with the leap-frog scheme. IUGG/IOC TIME Project, IOC manuals and guides, UNESCO, 35
- Gusman AR, Tanioka Y, Takahashi T (2012) Numerical experiment and a case study of sediment transport simulation of the 2004 Indian Ocean tsunami in Lhok Nga, Banda Aceh, Indonesia. *Earth Planets Space* 64:817–827
- Japan Nuclear Energy Safety Organization (2011) Cross-check analysis of the simulations of the 2011 Tohoku-Oki earthquake tsunami by the electric power company. <http://www.nsr.go.jp/archive/nisa/shingikai/800/26/003/3-4.pdf>. Retrieved on 2 Nov 2012
- Kotani M, Imamura F, Shuto N (1998) Tsunami run-up simulation and damage estimation by using GIS. *Proceedings of coastal engineering*. JSCE 45:356–360
- Matsumoto H (1985) Beach ridge ranges and the Holocene sea-level fluctuations on alluvial coastal plains, Northeast Japan. *Sci Rep* 35:15–46, Tohoku Univ., 7th series (geography)
- Okada Y (1985) Surface deformation due to shear and tensile faults in halfspace. *Bull Seismol Soc Am* 75(4):1135–1154
- Ozawa S, Nishimura T, Suito H, Kobayashi T, Tobita M, Imakiire T (2011) Coseismic and postseismic slip of the 2011 magnitude-9 Tohoku-Oki earthquake. *Nature* 475:373–376
- Richmond B, Szczuciński W, Chagué-Goff C, Goto K, Sugawara D, Witter R, Tappin DR, Jaffe B, Fujino S, Nishimura Y, Goff J (2012) Erosion, deposition and landscape change on the Sendai coastal plain, Japan, resulting from the March 11, 2011 Tohoku-Oki tsunami. *Sed Geol* 282:27–39. doi:10.1016/j.sedgeo.2012.08.005
- Szczuciński W, Kokociński M, Rzeszewski M, Chagué-Goff C, Cachão M, Goto K, Sugawara D (2012) Sediment sources and sedimentation processes of 2011 Tohoku-Oki tsunami deposits on the Sendai Plain, Japan – insights from diatoms, nannoliths and grain size distribution. *Sed Geol* 282:40–56. doi:10.1016/j.sedgeo.2012.07.019

- Takahashi T (2012) Numerical modeling of sediment transport due to tsunamis and its problem. *J Sed Soc Jpn* 71(2):149–155
- Takahashi T, Shuto N, Imamura F, Asai D (2000) Modeling sediment transport due to tsunamis with exchange rate between bed load layer and suspended load layer. *Proc Int Conf Coas Eng* 2000, Vol. 2, ASCE:1508–1519
- Takahashi T, Kurokawa T, Fujita M, Shimada H (2011) Hydraulic experiment on sediment transport due to tsunamis with various sand grain size. *J JSCE (J Seismol Coas Eng)* 67:231–235, Ser. B2 (Coastal Engineering)
- Tappin DR, Evans HM, Jordan CJ, Richmond B, Sugawara D, Goto K (2012) Coastal changes in the Sendai area from the impact of the 2011 Tohoku-Oki tsunami: interpretations of time series satellite images, helicopter-borne video footage and field observations. *Sed Geol* 282:151–174. doi:[10.1016/j.sedgeo.2012.09.011](https://doi.org/10.1016/j.sedgeo.2012.09.011)